Research Square

Preprints are preliminary reports that have not undergone peer review.
They should not be considered conclusive, used to inform clinical practice,
or referenced by the media as validated information.

Impact of Machine Learning on NMR-Based Permeability Prediction in Heterogeneous Carbonate Reservoir Analogs

Maurício Gabriel Lacerda Mafra

mauricio.mafra@ufrn.br

UFRN https://orcid.org/0000-0003-2720-4655

Milton Morais Xavier

UFRN

Research Article

Keywords: Nuclear Magnetic Resonance, Permeability prediction, Carbonate rocks, lithofacies, Machine learning

Posted Date: May 14th, 2026

DOI: https://doi.org/10.21203/rs.3.rs-9695238/v1

License: This work is licensed under a Creative Commons Attribution 4.0 International License.
Read Full License

Additional Declarations: The authors declare no competing interests.

Impact of Machine Learning on NMR-Based Permeability Prediction in Heterogeneous Carbonate Reservoir Analogs

Maurício Gabriel Lacerda Mafra, Post-Graduation Program on Geodynamics and Geophysics, Federal University of Rio Grande Do Norte, Natal, Brazil, mauricio.mafra@ufrn.br

Milton Morais Xavier, Post-Graduation Program on Geodynamics and Geophysics, Federal University of Rio Grande Do Norte, Natal, Brazil, milton.morais@ufrn.br

Abstract

Permeability prediction from Nuclear Magnetic Resonance (NMR) data remains challenging in carbonate rocks. Linear regression models, such as Schlumberger-Doll Research (SDR) and Han, rely on relatively homogeneous representations of the transverse relaxation time (T_2) distribution and often lose accuracy in carbonates affected by dissolution, fracturing, and karstification. This study compares the predictive performance of conventional regression models and supervised machine learning (ML) algorithms using exclusively NMR data. The analysis is based on a dataset of 494 carbonate core plugs collected from outcrop analogs of reservoir rocks from the Jandaíra Formation (Potiguar Basin, northeastern Brazil). Three ML algorithms, Random Forest Regressor (RFR), Gradient Boosting Regressor (GBR), and Multi-Layer Perceptron (MLP), were trained using T_2 distributions normalized by ϕ_{NMR}. Model training and evaluation were conducted using independent training and testing subsets, preserving lithofacies proportions. The results indicate that conventional models exhibit limited predictive capability, R^2 0.657 and σ_k 4.45, consistent with structural underfitting in highly heterogeneous carbonate systems, represented by distinct stratigraphic lithofacies with different behaviors and T_2 distributions. Ensemble-based ML models achieved robust fits to the training data but showed reduced performance on the test data. In contrast, the MLP model demonstrated superior generalization, lower prediction errors, R^2 0.759 and σ_k 3.5, and more stable residual behavior across the full permeability range. These findings highlight the importance of leveraging the full T_2 distribution for permeability modeling and demonstrate the potential of neural network-based approaches for characterizing complex carbonate reservoirs using NMR data.

Keywords: Nuclear Magnetic Resonance, Permeability prediction, Carbonate rocks, lithofacies, Machine learning

Introduction

Permeability is a fundamental petrophysical parameter for the evaluation of oil, gas, and water reservoirs. The direct measurement of permeability contributes to the optimization of reservoir use and management, influencing decisions at all stages, from exploration and prospecting to production and recovery (Kang et al. 2022; Lu et al. 2017; Rostami et al. 2022; Zhang et al. 2022). Absolute permeability values are obtained through in situ measurements or laboratory tests, mainly using core plugs (Darcy 1856; Sander et al. 2017; Tiab and Donaldson 2024). In many geological settings, permeability must be estimated using predictive models. This is mainly due to factors such as cost and time reduction, sampling limitations, accurate reservoir representation, and the possibility of real-time modeling. To ensure that these models properly represent the studied environment, a rigorous laboratory calibration process is required (Bi et al. 2023; Cipolla et al. 2010; Cipolla et al. 2008; Ling et al. 2014).

Within this context, Nuclear Magnetic Resonance (NMR) has become one of the most robust techniques in modern petrophysics, as it provides direct information on porosity and indirect information on pore space structure through the distribution of transverse relaxation times (T_2). These relaxation times reflect the interaction between fluids and pore surfaces and, under specific conditions, show correlation with pore and pore-throat size distributions, allowing inferences about connectivity and flow capacity (Chen et al. 2023a; Coates et al. 1999; Coates et al. 1998; Jensen et al. 2024; Kenyon et al. 1988; Liang et al. 2024; Wei and Zheng 2019). Based on these principles, several conventional multiple linear regression models have been proposed to estimate permeability from parameters derived from the T_2 distribution, including the Schlumberger-Doll Research (SDR) and Han models (Han et al. 2018; Kenyon et al. 1988).

Despite the success of these models, their application in more complex geological systems remains a significant challenge. In carbonate rocks, especially those affected by dissolution and karstification processes, pore space architecture is characterized by multiple interconnected scales, the coexistence of primary and secondary porosity, as well as fractures and conduits that introduce strong nonlinearities in hydraulic behavior. In this geological context, there is a lack of studies that achieve consistent success in permeability modeling, since the simplifying assumptions underlying conventional models, such as the dominance of a single relaxation regime or the representativeness of average parameters from the T_2 distribution, often no longer hold, leading to inaccurate or poorly robust estimates (Chang et al. 2023; Chencarek et al. 2019; Daigle and Dugan 2011; Elkatatny et al. 2018; Glover et al. 2006; J Al-Mudhafar 2019; Jin et al. 2019; Mahdaviara et al. 2020; Masroor et al. 2022; Otchere et al. 2022; Radwan et al. 2021; Souza et al. 2013; Zhao et al. 2024).

In parallel, advances in Machine Learning (ML) methods have significantly expanded the capability to model complex and nonlinear systems. Supervised algorithms, such as ensemble methods and artificial neural networks, are particularly suitable for

handling high-dimensional datasets and implicit relationships between variables, even in the absence of explicit linear correlations (Dong et al. 2020; Sagi and Rokach 2018). In petrophysics, recent ML applications have shown promising results for permeability estimation using NMR data; however, most of these studies remain limited to sandstones, synthetic data, or small sample sets, often evaluated only on the training dataset or without validation using independent data (Chen et al. 2023b; Kellal et al. 2026; Rezaee 2022; Zhu et al. 2017).

In addition, few studies systematically address lithostratigraphic complexity and how these depositional systems may exhibit wide pore–permeability variability, which can hinder modeling even when using ML approaches. This gap is particularly relevant in the context of Brazilian reservoirs, where carbonate rocks play a central role and petrophysical properties are strongly controlled by structural and diagenetic processes.

In this context, the present study aims to critically evaluate the performance of conventional and ML-based models for permeability prediction using exclusively NMR data, applied to a comprehensive dataset of 494 core plugs from a carbonate formation analogous to karstified reservoirs, encompassing different lithostratigraphic units. Specifically, this work seeks to: (i) compare widely used conventional models with different ML algorithms; (ii) employ independent training and testing subsets to assess model robustness and generalization capability; and (iii) quantitatively and interpretatively discuss the suitability of each approach for highly heterogeneous carbonate environments. By doing so, this study contributes to a more realistic understanding of the limitations and potential of permeability modeling based on NMR data in geologically complex settings.

Theory

Geology

The Potiguar Basin includes both onshore and offshore sectors, and its origin is related to the opening of the South Atlantic Ocean, which began during the Triassic–Jurassic, with the main rifting event occurring in the Cretaceous (~130 Ma). The stratigraphic record of the basin reflects its tectonic evolution, marked by the rift, transitional, and post-rift phases (Matos 1992; Neto et al. 2007). The Jandaíra Formation was deposited during the Albian post-rift phase, under a thermal subsidence regime associated with continental drift, and corresponds to a marine carbonate platform ranging from the Turonian to the Campanian. This unit is mainly composed of mudstones and bioclastic and intraclastic grainstones, with subordinate intercalations of sandstones, shales, marls, and evaporites, reaching a maximum thickness of approximately 600 m (Córdoba 2001; Neto et al. 2007).

The Jandaíra Formation was subjected to four main episodes of subaerial exposure, associated with Upper Turonian, Upper Santonian, and Upper Campanian unconformities, as well as late Cenozoic exhumation (Miocene–recent), resulting in intense karstification of the carbonate rocks (Bezerra et al. 2020; Neto et al. 2007; Silva

et al. 2017). These events were related to two post-rift stress fields: an older one, from the Late Cretaceous to the middle Miocene, characterized by N–S compression and E–W extension, and a more recent one, from the middle Miocene to the present, with regional variations in the compressional–extensional regime (Bagni et al. 2022; Bezerra et al. 2020). During the most recent event, the Apodi Folding developed, exerting strong structural and geomorphological control on the study area (Bagni et al. 2022; Lopes 2022). The carbonate rocks exhibit moderate primary porosity (~10%) and low permeability; however, the current petrophysical properties are dominated by secondary porosity and permeability associated with karst dissolution along bedding planes and fractures, within a predominantly epigenic karstification context and good outcrop preservation under a semi-arid climate (Araújo et al. 2021; Bagni et al. 2022; Fernandes et al. 2015; Silva et al. 2017).

The study area is located in outcrops of the Jandaíra Formation, in the western portion of the Potiguar Basin, situated along the equatorial Atlantic margin of northeastern Brazil (Fig. 1). The AT region was selected to observe the alternation between unaltered and altered rocks. The study aimed to represent transitions between non-altered and intensely karstified rocks in the AA region. The AFR region was selected to investigate areas with surface fractures and minimally altered layers. Within this context, the identified lithofacies include Grainstones, Bioturbated Grainstones, Wackstones, and Breached facies. A detailed description of each lithofacies, as well as thin-section examples, can be found in Lopes et al. (2023).

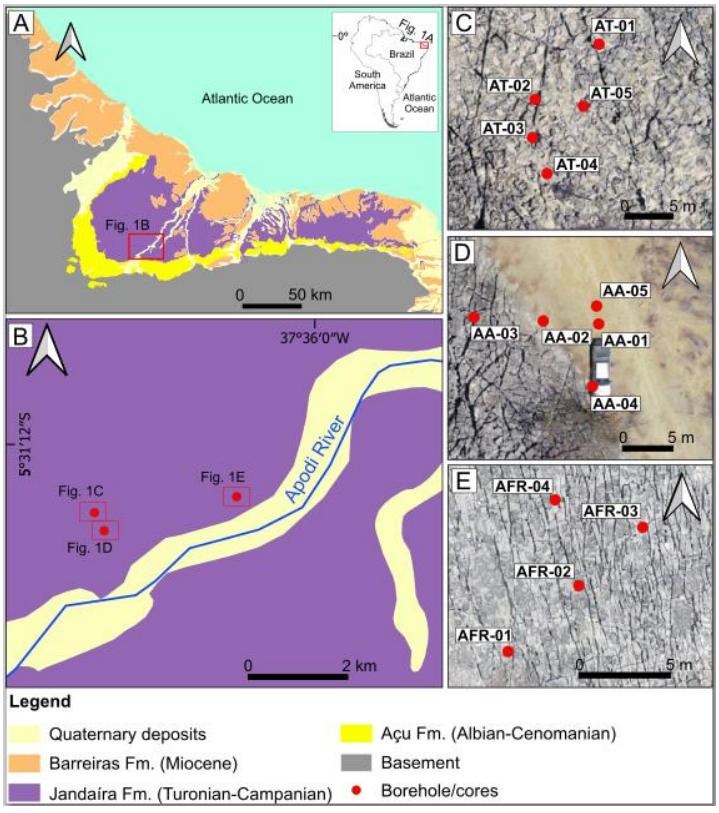


Figure 1 – a) Overview of the Potiguar Basin; b) Study area with the occurrence of karstified carbonates; c) AT study region; d) AA study region; e) AFR study region.

Techniques and Applications of Nuclear Magnetic Resonance

Nuclear Magnetic Resonance (NMR) is a well-established tool in petrophysics, as it allows the characterization of the porous medium based on the response of the nuclear spins of hydrogen atoms present in the fluids occupying the rock pores. In petrophysical applications, the information of greatest interest is the transverse magnetization, whose temporal evolution reflects the relaxation mechanisms associated with interactions between the fluids, the pore surfaces, and the applied magnetic field.

The acquisition of T_2 is performed using Carr–Purcell–Meiboom–Gill (CPMG) pulse sequences (Fig. 2a–b) (Carr and Purcell 1954; Hahn 1950; Meiboom and Gill 1958), which allow recording the decay curve of the transverse magnetization as a function of time (Fig. 2c). This curve represents the superposition of multiple relaxation processes associated with different pore environments and confinement scales. Mathematically, the effective transverse relaxation time (T_2) can be expressed as the sum of contributions related to the bulk fluid properties, surface relaxation, and diffusion effects in non-uniform magnetic fields (Dunn et al. 2002):

$$\frac{1}{T_2} = \frac{1}{T_{2\,B}} + \frac{1}{T_{2\,S}} + \frac{1}{T_{2\,D}} \tag{1}$$

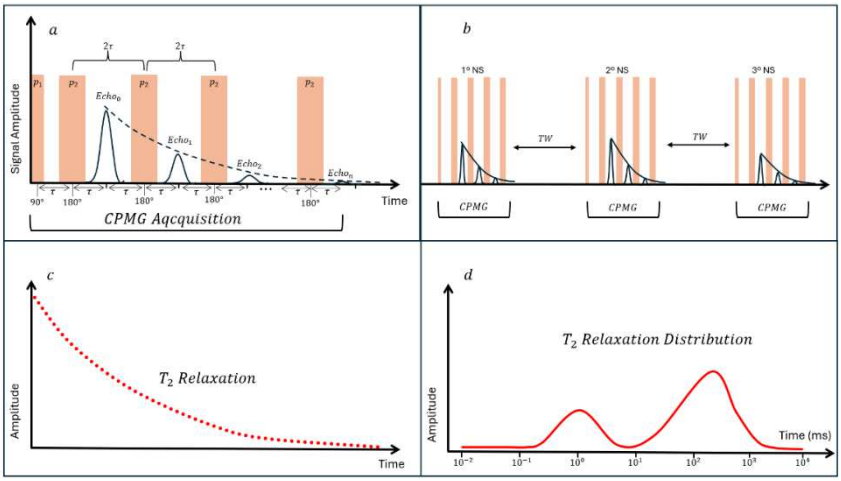


Figure 2 - a) CPMG pulse sequence; b) CPMG sequences for relaxation time acquisition; c) T_2 relaxation curve; d) T_2 relaxation distribution

In porous systems saturated with low-viscosity fluids and under typical laboratory NMR experimental conditions, surface relaxation (T_{2S}) tends to dominate when the pore surface-to-volume ratio is high. Under these conditions, the T_2 time becomes approximately proportional to the characteristic pore size, establishing an indirect relationship between the relaxation time distribution and the distribution of pore and throat sizes (Coates et al. 1999). The transverse magnetization decay curve is converted into a T_2 relaxation time distribution through mathematical inversion (Fig. 2d), usually formulated as an ill-posed inverse problem. The solution of this problem requires the introduction of regularization terms, since it is ill-posed and therefore demands the

imposition of smoothness or stability on the obtained distribution (Dunn et al. 2002; Tikhonov and Arsenin 1963). These effects, however, can be minimized using iterative methods, such as the Simultaneous Iterative Rebuild Technique (SIRT) (Chen et al. 2010). Although the T_2 distribution does not represent a unique description of the pore space geometry, it provides a robust statistical representation of the different pore populations contributing to the NMR signal, as long as the acquisition and inversion conditions are kept consistent.

The validity of conventional NMR-based permeability prediction models, such as the Schlumberger–Doll Research (SDR) model (2) and the model proposed by Han et al. (2018) (3), is strongly associated with the implicit assumption that surface relaxation dominates the relaxation regime and that the T_2 distribution can be adequately described by average parameters or by predefined fractions of the spectrum (Han et al. 2018; Kenyon et al. 1988). In the Han model, the T_2 distribution is partitioned into four time intervals: S_1 ($T_2 \leq 30$ ms), S_2 (30 ms $< T_2 \leq 90$ ms), S_3 (90 ms $< T_2 \leq 200$ ms), and S_4 ($T_2 > 200$ ms), which are interpreted as representative of pores at different scales, ranging from micropores and strongly confined pores (S_1 and S_2) to larger and better-connected pores, potentially dominant in fluid flow (S_3 and S_4). This assumption is often satisfied in relatively homogeneous clastic rocks, in which pore space connectivity is controlled by a limited range of scales and the T_2 distribution exhibits unimodal or weakly multimodal behavior (Chang et al. 2023; Chencarek et al. 2019; Daigle and Dugan 2011; Glover et al. 2006; Jin et al. 2019; Liu et al. 2019; Masroor et al. 2022; Rezaee 2022; Souza et al. 2013; Xu et al. 2020).

$$k_{SDR} = a \cdot {T_{2\,lm}}^{b} \cdot {\phi_{NMR}}^{c} \tag{2}$$

$$k_{Han} = a \cdot {\phi_{NMR}}^{b} \cdot \frac{{S_3}^{c} \cdot {S_4}^{d}}{{S_1}^{e} \cdot {S_2}^{f}} \tag{3}$$

In carbonate rocks, however, this condition is rarely met. The coexistence of primary and secondary porosity, associated with dissolution, fracturing, and karstification processes, results in highly hierarchical pore space architectures with multiple interconnected scales (Araújo et al. 2021; Lopes et al. 2023; Yu et al. 2020; Zhao et al. 2017). In such systems, different relaxation regimes may coexist, and the T_2 distribution tends to be broad and strongly multimodal, reflecting not only variations in pore size but also differences in hydraulic connectivity and flow accessibility. As a consequence, reducing the T_2 distribution to average parameters or fixed fractions may lead to the loss of information relevant to fluid transport, thereby compromising the predictive capability of conventional models. This physical limitation provides the conceptual basis for adopting alternative approaches, such as those based on machine learning (ML) algorithms, which can exploit the full T_2 distribution and its nonlinear relationships with permeability, especially in highly heterogeneous carbonate environments.

Machine Learning Algorithms and Applications

As machine learning (ML) algorithms are able to perform tasks without being explicitly programmed (Samuel 1959), they allow researchers to handle multidimensional and heterogeneous datasets without requiring predefined correlations among variables. This provides a flexible and powerful approach for extracting meaningful information (Géron 2021; Pedregosa et al. 2015). However, as noted by Wolpert (1996), each ML problem has unique characteristics, and therefore there is no universal model nor a simple way to determine the ideal algorithms and parameters to solve it. In this context, it is recommended to apply more than one ML algorithm using different hyperparameter settings in order to identify the most efficient model for the problem under investigation. Supervised algorithms widely used in nonlinear regression problems include ensemble methods and neural networks, such as Random Forest Regressor (RFR), Gradient Boosting Regressor (GBR), and Multi-Layer Perceptron (MLP) (Géron 2021; Pedregosa et al. 2015).

Ensemble-based models, such as RFR and GBR, rely on the combination of multiple decision trees, exploring different subsets of samples and input variables in order to reduce variance and improve prediction stability. To capture different aspects of the dataset, random sampling with replacement, known as bootstrap, is applied, allowing repeated samples to be evaluated by different trees that consider only subsets of the input variables. This strategy aims to diversify decision paths and reduce overfitting. In Random Forest, trees are trained independently using bootstrap sampling and random feature selection (Biau and Scornet 2016; Breiman 2001; Liu et al. 2012; Sagi and Rokach 2018; Segal 2003), whereas in Gradient Boosting, trees are constructed sequentially to correct the residuals of previous iterations through the minimization of a loss function (Bentéjac et al. 2021; Friedman 2001; Mayr et al. 2014; Natekin and Knoll 2013). These approaches are particularly effective in identifying local patterns in the data, but their generalization capability may degrade when applied to highly heterogeneous datasets with limited sample size.

The neural network model MLP combines data processing units arranged in networks that can be connected laterally and in depth (Jain et al. 1996; McCulloch and Pitts 1943). These units, known as perceptrons, are composed of activation functions and weights, and the training process is performed through error backpropagation, which automatically adjusts these coefficients using gradient-based calculations over successive epochs (Braga et al. 2011; Haykin 2009; Hinton and Osindero 2006). This architecture enables the modeling of highly nonlinear relationships between input variables and target values, without imposing explicit assumptions about the functional form of these relationships.

All algorithms can assume a wide variety of different architectures, potentially leading to an infinite number of models. These architectures are defined by a set of hyperparameters that shape the model structure and behavior, directly influencing its ability to capture complex patterns in the data. Hyperparameters correspond to prior information provided to the algorithms, allowing them to produce the best possible predictions, such as controlling the number of trees or perceptrons. For this reason, in this

study, all algorithms were trained using systematic hyperparameter optimization through the GridSearchCV method, which performs training over a predefined hyperparameter grid for a given algorithm and automatically applies cross-validation to the training data in order to identify the best hyperparameter combination according to a selected metric.

The comparison between conventional regression models and machine learning algorithms introduces additional challenges in performance evaluation, since these approaches differ substantially in structural complexity, effective number of parameters, and regularization mechanisms. Consequently, the most commonly used metrics for evaluating both linear regressions and ML models are R^2 (4) and RMSE (5), since they are based solely on the comparison of residuals (6), which are obtained independently of the type of model adopted.

$$R^2 = 1 - \frac{\sum({y_{real}}^{(i)} - {y_{predicted}}^{(i)})^2}{\sum({y_{real}}^{(i)} - \bar{y}_{real})^2} \tag{4}$$

$$RMSE = \sqrt[2]{\frac{1}{N}\sum_{i=1}^{N}[{y_{real}}^{(i)} - {y_{predicted}}^{(i)}]^2} \tag{5}$$

$$Residuals = y_{real} - y_{predicted} \tag{6}$$

Materials and Methods

Sample and Data Acquisition

For data acquisition, 14 well drillings were carried out, each with an approximate depth of 10 m, distributed across three distinct regions of the Jandaíra Formation: AA, AT, and AFR (Fig. 2c–e). Plugs were obtained by lateral drilling of the cores at depth intervals of approximately 20 cm. These samples have a diameter of 25 mm and a maximum height of 50 mm, totaling 494 units. Examples of the different lithofacies include bioturbated, brecciated, grainstones, and wackstones (Fig. 3a–d).

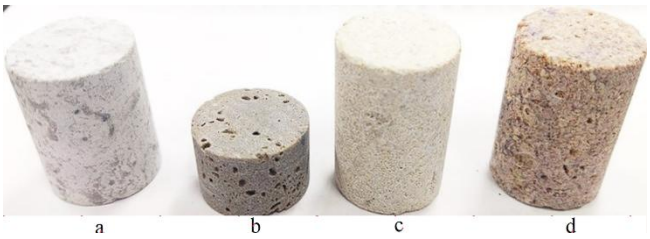


Figure 3 - Representation of each lithofacies in some plugs: a) bioturbated, b) breached, c), grainstone and d) wackstone.

Porosity and gas permeability measurements were performed on these plugs using a gas overburden porosimeter and an unsteady-state gas permeameter, employing nitrogen gas under a confining pressure of 600 psi. The Klinkenberg correction was applied to adjust the unsteady-state gas permeability (Araújo et al. 2021; Klinkenberg 1941; Lopes et al. 2023). The NMR equipment used in this study was the Niumag MesoMR12-060H-I, which is accompanied by software that assists the user in selecting global parameters for CPMG sequence acquisition, as well as controlling signal gain and noise reduction, resulting in high-resolution signals (Table 1).

Table 1 - Parameters for obtaining relaxation curves

Parameters	**τ(ms)**	**NECH**	**TW (ms)**	**NS**	**PGR**
Value	*0.200*	*18000*	*10000*	*16*	*1*

To minimize user influence on obtaining the T_2 relaxation time distribution curve, the SIRT optimization method was used for the inversion, with a maximum number of 10,000 iterations. The inversion was performed using 128 bins over a time range from 0.01 to 10,000 ms. Subsequently, the area under the T_2 distribution curve was normalized to represent ϕ_{NMR}. This dataset was then randomly divided into two independent subsets while preserving lithofacies proportions: 70% of the samples from each lithofacies were used for training and 30% for testing. In total, 344 samples were used for training and 150 for testing.

Metrics

The comparison of porosity obtained by different techniques aims to verify whether both data subsets are equivalent. The RMSE, denoted as σ_ϕ, was used to represent this error based on porosity data and is expressed in porosity units (p.u.). The R^2 parameter was used by GridSearchCV to determine the best set of trained hyperparameters, in agreement with the literature. Due to the large variability in permeability, ranging from 10^{-3} to 10^4 mD, the RMSE was normalized (Eq. 7) and denoted as σ_k to represent the error associated with permeability data.

$$log_{10}(\sigma_k) = \sqrt[2]{\frac{1}{N}\sum_{i=1}^{N}[log_{10}({k_{model}}^{(i)}) - log_{10}({k_{gas}}^{(i)})]^2} \quad (7)$$

The evaluation of the performance of the algorithms and models in this study was based on an explicit analysis of their generalization capability, through the comparison of R^2 and σ_k errors obtained from independent training and testing subsets. The best ML model was defined as the one that achieved the lowest σ_k error in the test dataset (σ_k-Test).

Training and Regression

The choice of the algorithms, RFR, GBR, and MLP, was based on their proven ability to handle high-dimensional datasets and complex nonlinear relationships, as

demonstrated in several fields of scientific research, including petrophysics (Astsauri et al. 2024; Gonçalves et al. 2017; Henrique et al. 2019; Mahesh 2020; Masroor et al. 2022; Prieto-González and Agulles-Pedrós 2023; Sun et al. 2022; Zhang and Haghani 2015; Zounemat-Kermani et al. 2021). This approach ensures that the observed differences among models reflect not only algorithmic variations, but also each method's ability to exploit the informational content of the T_2 distribution in complex carbonate environments.

The training of these algorithms was performed using GridSearchCV with a five-fold cross-validation scheme. The model selection criterion was the highest R^2 value, ensuring consistency when comparing models with different architectures (Appendix A) (Alhakeem et al. 2022; Pedregosa et al. 2015). After defining the optimal set of hyperparameters, each model was independently evaluated on the training and test subsets, allowing an explicit analysis of predictive performance and generalization capability using the R^2 and σ_k metrics (Appendix B).

Conventional models need to be linearized through the application of the $\log_{10}$ transformation, namely the SDR (Eq. 8) and Han (Eq. 9) models. The coefficients of each model are obtained by RLM applied to the training dataset (Chen et al. 2023b; Han et al. 2018; Kenyon et al. 1988), using their respective parameters, such as T_{2lm}, S_1, S_2, S_3, S_4, and ϕ_{NMR}. Once the coefficients of each model are obtained (Appendix B), predictions can be performed on both data subsets, and accuracy and error metrics can be computed.

$$\log(k_{SDR}) = \log(a) + b \cdot \log(T_{2\,lm}) + c \cdot \log(\phi_{NMR}) \quad (8)$$

$$\log(k_{Han}) = \log(a) + b \cdot \log(\phi_{NMR}) + c \cdot \log(S_3) + d \cdot \log(S_4) - e \cdot \log(S_1) - f \cdot \log(S_2) \quad (9)$$

Workflow

Therefore, this research was conducted using a multidisciplinary approach that includes: the use of different ML algorithms and their comparison with conventional models; the incorporation of lithostratigraphic descriptions in the separation of training and test datasets; and the development of an evaluation metric to compare ML and RL models. The workflow is shown in Fig. 4 and starts with the acquisition of geological and petrophysical data, followed by permeability modeling using ML and RL approaches, and the comparison of model performance.

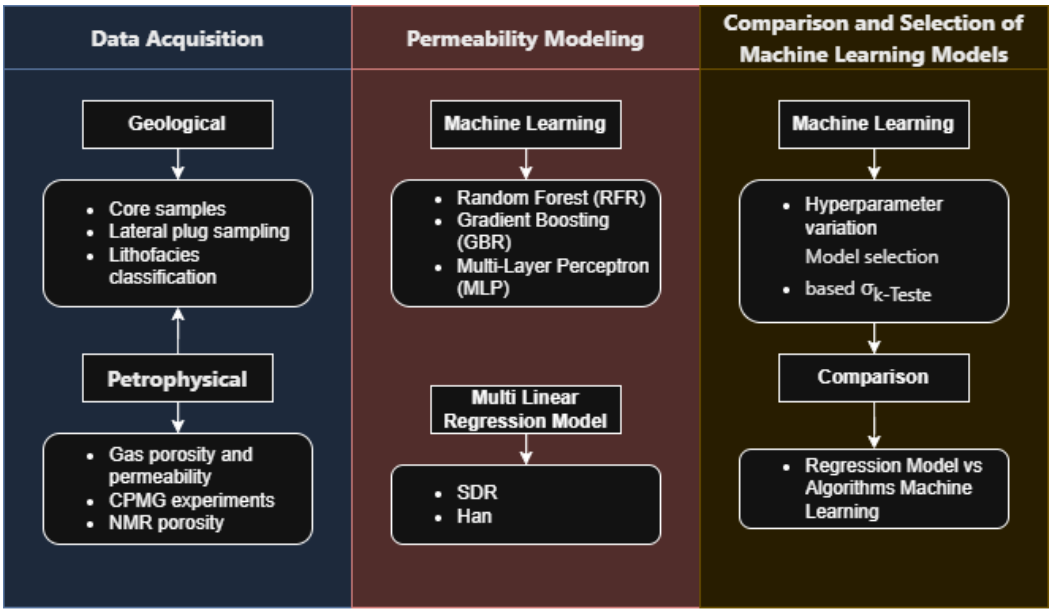


Figure 4 – Workflow for petrophysical data acquisition, permeability modeling using ML algorithms and conventional regression models, and model comparison.

Results

The dataset was divided into training and testing subsets in order to ensure a statistically robust evaluation of the models, while maintaining a proportional distribution of lithofacies between the subsets (Table 2). A predominance of Grainstone and Wackstone lithofacies is observed, which together account for approximately 80% of the samples, whereas Bioturbated and Breached facies are less frequent.

Table 2 - Number of samples in each lithofacies

Lithofacies	Training	Test
Grainstone	177	74
Wackstone	99	44
Breached	36	17
Bioturbated	32	15

The average petrophysical results, as well as the comparison between the different techniques for each lithofacies, are summarized in Table 3. Although Grainstone and Wackstone are the dominant lithofacies, they exhibit extreme petrophysical differences, presenting the highest and lowest porosity and permeability values, respectively. In contrast, the Bioturbated and Breached facies show more balanced and relatively similar values. When evaluating the proportions of the T_2 distribution, the S_1 and S_2 fractions, associated with smaller pores, show systematically lower mean values in the Grainstone and Breached lithofacies, whereas Wackstone and Bioturbated display higher fractions, indicating a T_2 distribution shifted toward shorter relaxation times. This behavior reveals a strong similarity between Grainstone–Breached and, analogously, between Wackstone–Bioturbated, suggesting that NMR captures aspects of pore-space connectivity and hierarchy that are not evident from conventional petrophysical analysis. Therefore, maintaining similar proportions between the subsets ensures that the model evaluation is

not biased by statistical differences in lithostratigraphic composition, allowing more consistent comparisons between training and testing performance.

Table 3 - Presentation of experimental results, evaluating the average values for each lithofacies. The analyzed parameters include gas permeability, as well as Gas and NMR porosity. From the time distribution, T_{2lm} and fractions S_1, S_2, S_3, and S_4 are obtained, along with the coefficients R^2_ϕ, and σ_ϕ, which quantify the relationship between NMR values and Gas data.

Lithofacies	Average								R^2_ϕ	σ_ϕ
	ϕ_{Gas}	ϕ_{NMR}	$T_{2\,lm}$	S_1	S_2	S_3	S_4	k_ϕ		
Bioturbated	11.8	11.4	10.1	85.1	13.7	0.8	0.4	0.172	0.93	±1.12
Breached	11.9	10.6	29.9	53.6	36.6	6.0	3.7	0.436	0.87	±1.90
Grainstone	15.3	14.7	40.1	45.8	37.3	11.3	5.6	3.914	0.84	±1.89
Wackstone	8.0	7.5	9.7	88.7	7.5	1.8	2.0	0.080	0.62	±1.70

These differences are visually evident in Figure 5, which presents the gas porosity and NMR porosity values for the Training and Test subsets (Fig. 5a–b), together with the individual lithofacies distributions within each subset (Fig. 5c–j).

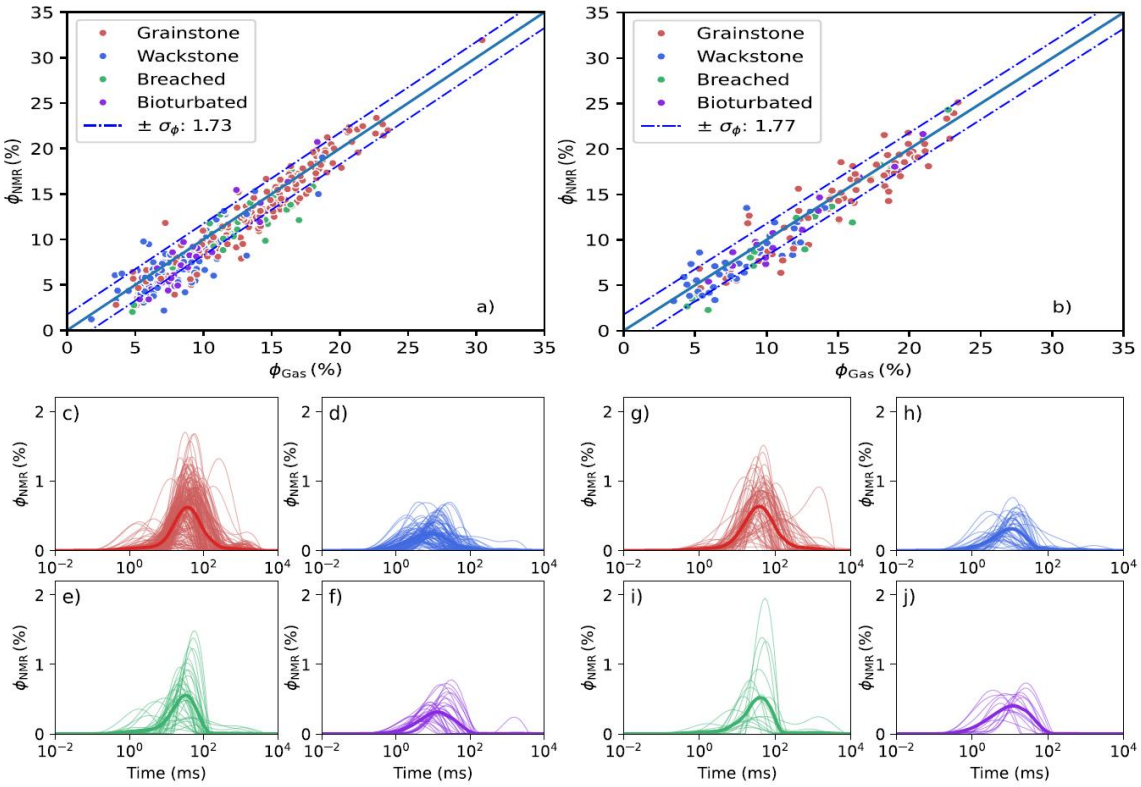


Figure 5 – Comparison between gas porosity and NMR data**.** a–b) Training and test sets; c–d) T_2 time distributions for the training dataset with lithofacies identification and highlighted average curves; g–h) T_2 time distributions for the test dataset with lithofacies identification and highlighted average curves. Lithofacies represented: grainstone (c, g), wackestone (d, h), breached (e, i), and bioturbated (f, j).

The permeability predictions of the ML models, RFR, GBR, and MLP, on the Test subset are shown in Figure 6, bounded by $\sigma_{k\text{-Test}}$. The RFR model shows poorer performance for permeabilities above 10^2 mD, while maintaining good agreement below

this threshold. In contrast, the GBR and MLP models demonstrate higher accuracy across the entire permeability range, resulting in σk values lower than those obtained with RFR.

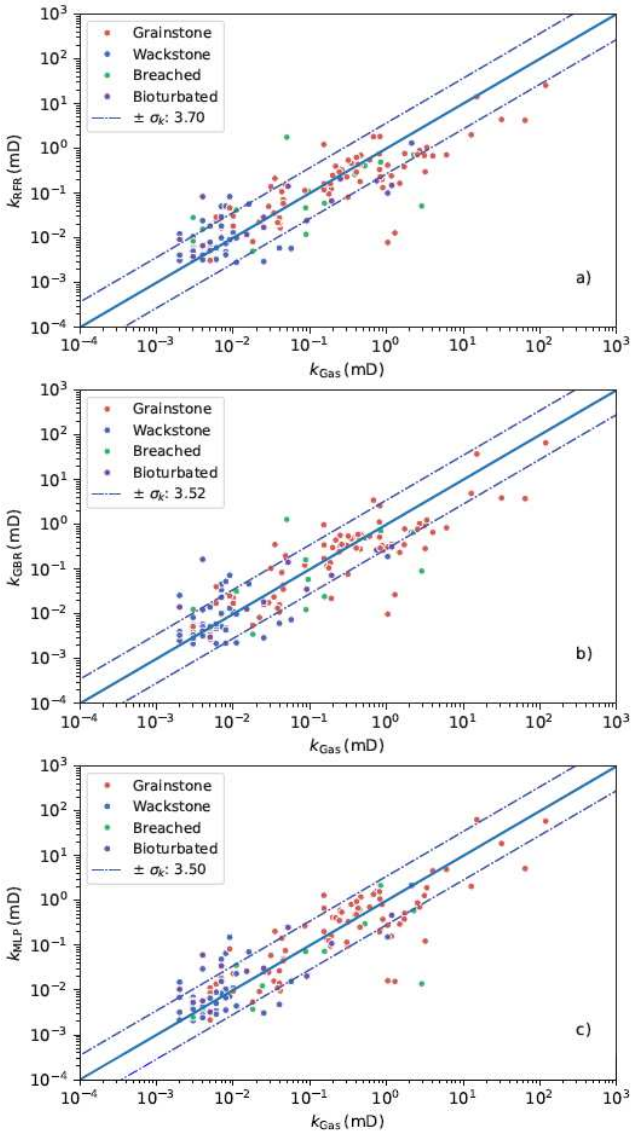
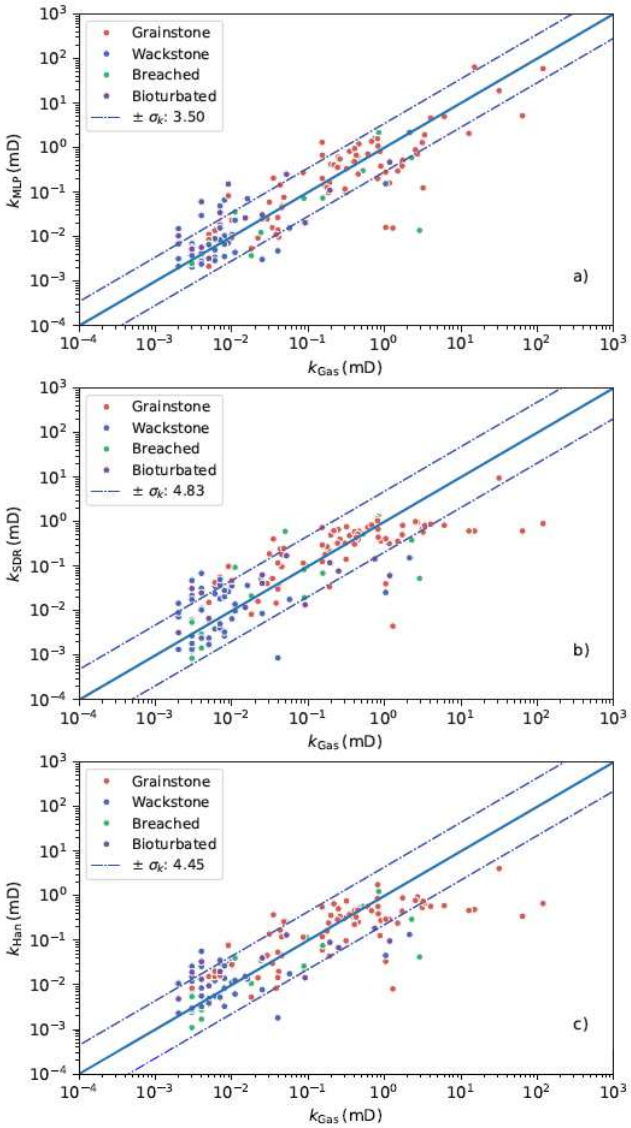


Figure 6 - Evaluation of permeability predictions from gas data using the algorithms with Test data: a) RFR; b) GBR; c) MLP.

Considering the $\sigma_{k\text{-Test}}$ criterion to determine the best performance of the ML algorithms, with the aim of comparing them with the conventional models, SDR and Han, and evaluating the overall accuracy of the methods, it is observed (Fig. 7) that the MLP model presents the best agreement across all permeability ranges. The conventional models exhibit pronounced errors at very high (>100 mD) and very low ($<10^{-2}$ mD) permeabilities, deviating from the measured values. At low permeabilities, between 0.001 mD and 0.009 mD, a quantization effect occurs due to the experimental resolution on the order of 10^{-3} mD. This scaling produces a visual artifact that reflects the limitation of laboratory data resolution; however, it can be mitigated by the models, since they allow

continuous estimates within this range. Even under this condition, the MLP model maintains good agreement.



.Figure 7 - Evaluation of permeability predictions from gas data using the algorithms with Test data: a) MLP; b) SDR; c) Han.

Table 4 presents the global comparison between the experimental mean values and those estimated by the evaluated models, for both the Training and Test subsets. The coefficients of determination (R^2), the errors associated with porosity (σ_ϕ) and permeability (σ_k) estimates are analyzed. The values associated with the experimental properties (ϕ_{Gas} and k_{Gas}) are shown as reference; therefore, they exhibit unitary R^2 and null error. The porosity estimated by NMR shows excellent agreement with gas porosity, with R^2 values higher than 0.87 in both subsets and σ_ϕ errors on the order of ±1.7 p.u., confirming the robustness of the technique.

Regarding permeability estimation, the conventional SDR and Han models present the lowest R^2 and the highest σk among all evaluated models. It is also observed that, during training, both R^2 and σk are worse than those obtained in the test subset.

Compared with the other models, this behavior can be interpreted as underfitting. The RFR and GBR algorithms exhibit excellent fits in the Training subset, with R^2 values above 0.95 and low σ_k values. However, when applied to the Test subset, a significant degradation in performance is observed, with a reduction in R^2 and a pronounced increase in σ_k, which may indicate overfitting. The MLP algorithm shows a balanced behavior, with similar R^2 and σ_k values in both Training and Test subsets, ruling out both underfitting and overfitting, even though it presents the best overall R^2 and σk metrics. This behavior further supports the absence of overfitting and underfitting, since the errors remain subtle when compared to the other algorithms.

Table 4 - Presentation of the average porosity and permeability for each model, assessing both training and test data sets. The evaluation includes the relationship between each estimate and gas permeability, quantified through R^2 and σ.

	Average		R^2		σ_ϕ **or** σ_k	
	Train	**Test**	**Train**	**Test**	**Train**	**Test**
$\boldsymbol{\phi_{Gas}}$ **(p.u)**	11.71	12.44	1	1	0	0
$\boldsymbol{\phi_{NMR}}$ **(p.u)**	10.87	11.79	0.875	0.887	±1.73	±1.77
$\mathbf{k_{Gas}}$ **(mD)**	39.96	61.05	1	1	1	1
$\mathbf{k_{SDR}}$**(mD)**	39.96	61.05	0.524	0.618	5.24	4.83
$\mathbf{k_{Han}}$ **(mD)**	39.96	52.29	0.571	0.657	4.82	4.45
$\mathbf{k_{RFR}}$ **(mD)**	39.85	54.67	0.951	0.737	1.71	3.70
$\mathbf{k_{GBR}}$ **(mD)**	36.96	52.55	0.954	0.756	1.67	3.52
$\mathbf{k_{MLP}}$ **(mD)**	40.82	56.79	0.779	0.759	3.09	3.50

The residual analysis performed on the Test subset (Fig. 8) reinforces the superiority of the MLP model over the conventional models. Its residual distribution (Fig. 8a) approaches a narrower Gaussian shape, with a higher density of errors concentrated near zero. In the residual map (Fig. 8b), the MLP model exhibits a homogeneous behavior across the entire permeability range, with a high density of residuals close to zero, including both high and low-permeability intervals. In contrast, the conventional models show a residual pattern with a positive linear trend, indicating increasing errors toward more extreme permeability values, both high and low. The Han model, although presenting a high density of residuals in the low-permeability range, does not show a distribution centered at zero, evidencing a systematic bias.

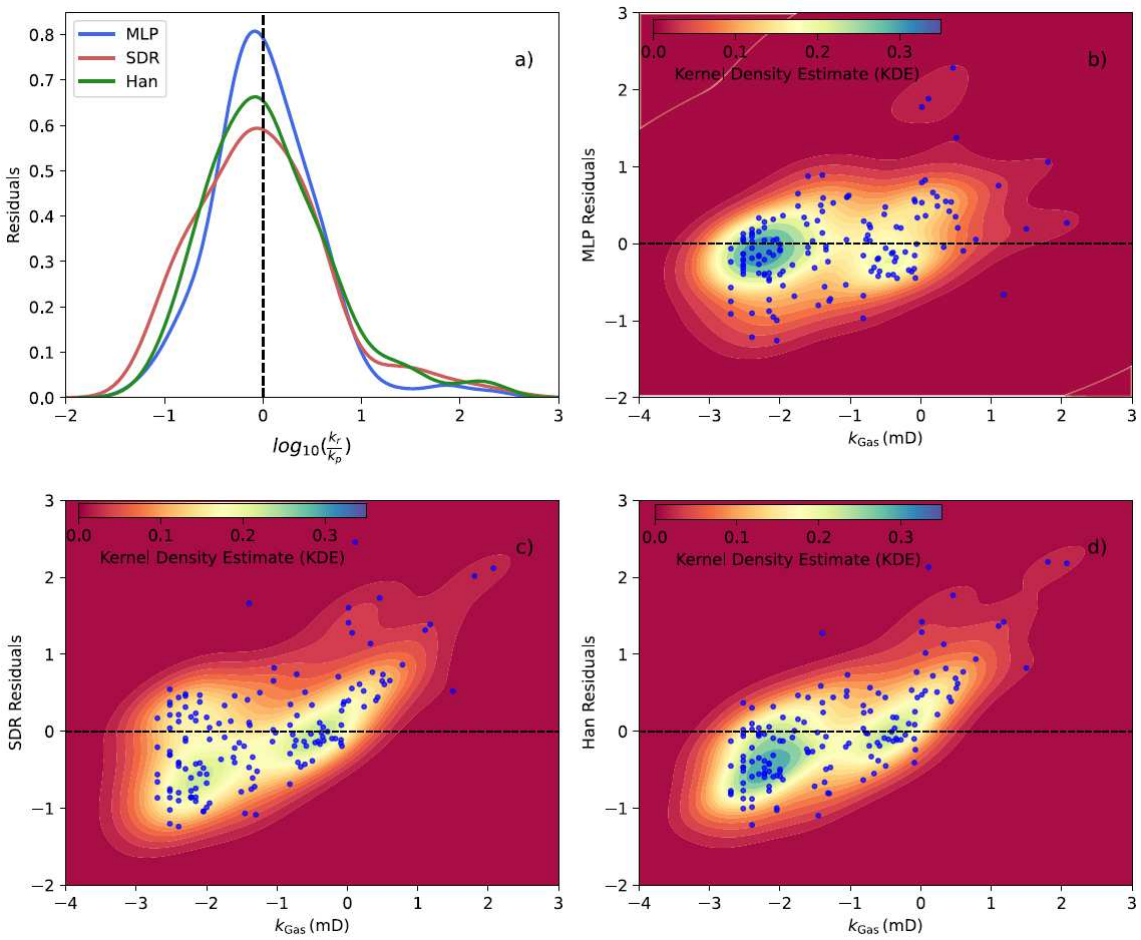


Figure 8 - Residual analysis on the test subset: (a) the residual distribution for the MLP, SDR, and Han models; residual maps for the models (b) MLP, (c) SDR, and (d) Han.

The lithostratigraphic description of all samples from well AFR2, together with laboratory-measured permeability and the results obtained from the most promising models, MLP and Han, as well as the T_2 distributions, are presented in Figure 9. A clear difference in model accuracy is observed, particularly in intervals with higher permeability. This behavior highlights how the complexity of well-log data directly influences algorithm performance and how the NMR response reflects this same complexity. NMR captures variations related to pore texture, which are clearly expressed in the T_2 distributions and may be associated with permeability estimation. However, conventional predictive models, which rely only on selected information from the distribution, show inherent limitations. In contrast, the MLP-based approach demonstrates greater adaptability, although it also faces challenges.

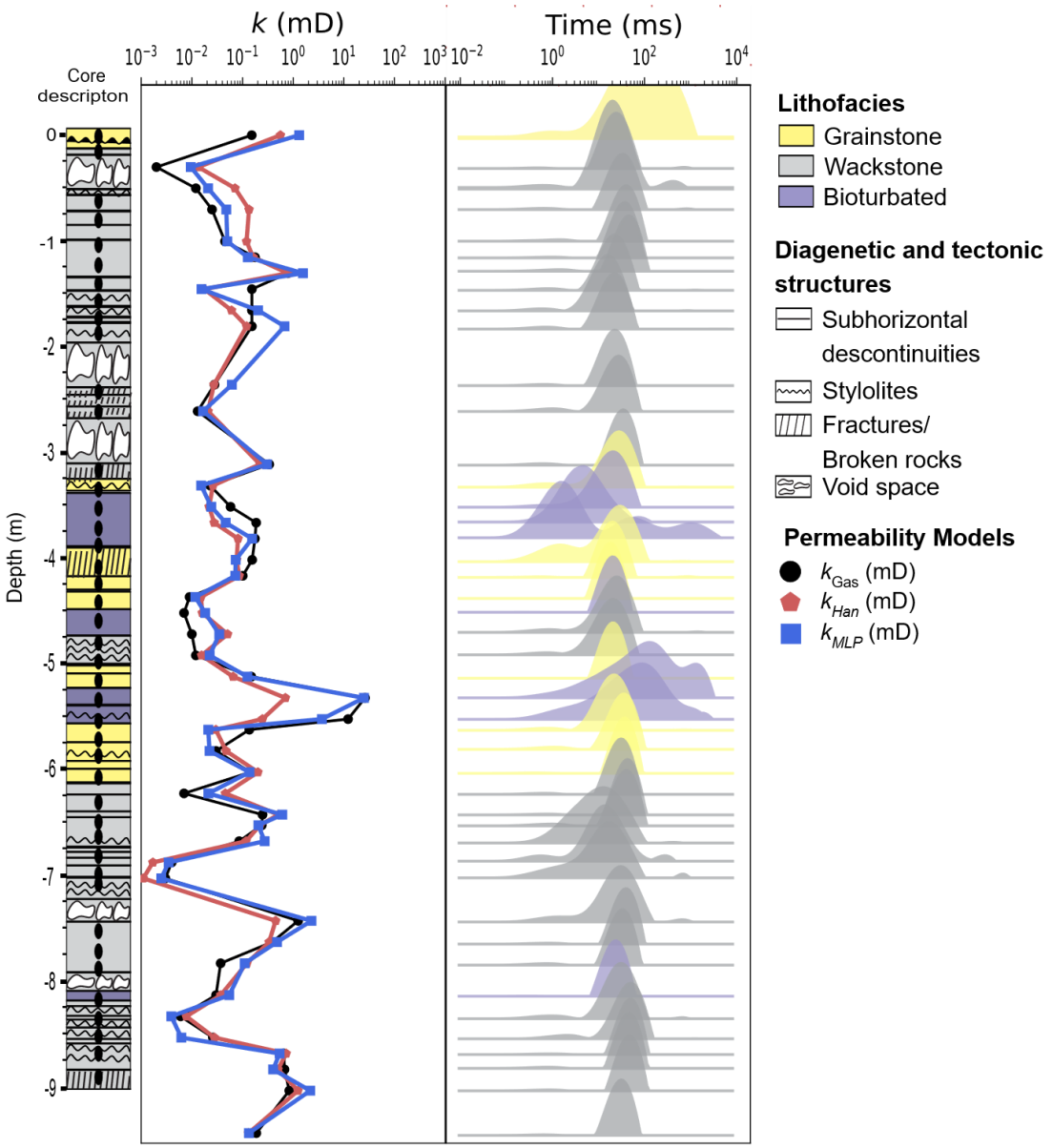


Figure 9 - AFR2 borehole profile showing lithofacies, laboratory gas permeability, permeability estimates from the MLP and Han models, and corresponding NMR T_2 relaxation time distributions.

Discussions

The choice of a complex geological setting was essential to show that carbonate rocks are rarely dominated by a single T_2 relaxation regime. In this context, the results support the hypothesis that different lithofacies may exhibit similar T_2 responses when they share comparable pore-space architectures. The similarity observed between Grainstone and Breached suggests more open and better-connected pore domains, whereas the correspondence between Wackstone and Bioturbated indicates a stronger contribution of microporosity and pores with smaller effective sizes, consistent with a shift of the T_2 distribution toward shorter values. This distribution reflects the natural heterogeneity typical of carbonate reservoirs and poses an additional challenge for modeling, since models must be able to capture consistent petrophysical patterns even in

under-represented lithofacies. This behavior is consistent with recurring observations reported in the NMR literature applied to heterogeneous carbonates and karst systems (Araújo et al. 2023; Lopes et al. 2023; Lopes 2022).

Although Grainstone and Wackstone are predominant in the dataset, this asymmetry was not a determining factor in the study results, since the permeability values covered by these two lithofacies span the entire range, particularly the extreme values. Therefore, lithostratigraphic descriptions were not used as model inputs, but only as interpretative support and as a criterion for data separation. When the T_2 distributions are analyzed, these lithofacies show nearly two classes: those with distributions shifted toward shorter relaxation times and those shifted toward longer times. This shift clearly separates Grainstone from Wackstone, providing deeper insights into the heterogeneity of pore structure across different lithofacies, which is critical for reservoir modeling. Consequently, models that do not incorporate a broader set of NMR-derived information may fail to fully capture these nuances.

By respecting geological criteria in data separation, the models become more representative of real reservoir scenarios. Model training using GridSearchCV was effective, as it enabled the optimization of several different models using R^2 as the evaluation metric, which is the most commonly adopted criterion in ML studies. The subsequent use of σ_k is also appropriate for model evaluation, as it was originally proposed by Kenyon et al. (1988) for assessing the SDR model and provides a robust measure of model accuracy even across a wide range of permeability values.

The complexity of the dataset can be assessed by comparing the results obtained in this study with those reported in the literature for conventional models. Souza et al. (2013) and Han et al. (2018), when applying the SDR model to their sample sets, reported R^2 values of 0.80 and 0.81, respectively, while the Han model itself achieved an R^2 of 0.93. Kellal et al. (2026) showed that, when their data were applied to the SDR model, the resulting fit yielded R^2 0.52. In the present study, these same models yielded R^2 values of 0.52 and 0.57 (Table 4) on the training data, confirming that the sample set is more complex. Regarding the σ_k error, previous studies on sandstones (Chen et al. 2023a; Kenyon et al. 1988) reported values of 2.65 and 3.1, respectively, for the SDR model. In this work, σ_k values for the SDR model reached 5.24 and 4.84 for the training and test datasets (Table 4). These findings reinforce the evidence that permeability modeling in carbonates is substantially more challenging than in sandstones, justifying the need for larger datasets than those typically used in earlier studies and indicating that further investigations are still required in complex geological settings.

Due to the limited number of studies focused exclusively on permeability estimation from NMR data, comparisons between the results obtained here and ML-based approaches can only be made partially. Zhu et al. (2017) and Chen et al. (2023a) applied ML models to sandstone samples using 200 and 123 samples, respectively. Among these studies, only Chen et al. (2023a) reported R^2 values for the test datasets, obtaining 0.8446 and 0.8194 for the GBR and RFR models, respectively. In the present work, using the

same algorithms, the corresponding R^2 values were 0.756 and 0.737 (Table 4). As discussed earlier, the higher complexity of the dataset analyzed here explains the larger estimation errors. In addition, previous studies did not report σ_k error metrics for the training and test datasets, which makes it difficult to assess the degree of model generalization.

The study by Kellal et al. (2026) evaluated Ensemble algorithms and an MLP using distinct training and testing datasets, applied to a relatively large database composed of sandstone and carbonate samples. Different input data configurations were investigated, including bins of the T_2 distribution, and test determination coefficients on the order of R^2 0.85 for XGB and R^2 0.82 for MLP were reported. Despite the overall good performance achieved by Kellal et al., the study does not explicitly discuss behavioral differences between sandstones and carbonates, nor does it provide a detailed assessment of how lithological heterogeneity influences prediction errors. This lack of stratified analysis limits the interpretation of the results and hampers direct comparison with the present work, in which the greater dataset complexity and the joint evaluation of training and testing metrics reveal additional generalization challenges that are not fully addressed in previous studies.

With the aid of the residual error maps (Fig. 8), it is possible to observe a typical characteristic of conventional predictive models: their tendency to model a global average at the expense of extreme permeability values. These models rapidly lose coherence as permeability increases or decreases relative to the global mean, which compromises petrophysical interpretation. This behavior is further illustrated in Fig. 9, where intervals of well AFR2 that contain high-permeability zones are not properly captured by the conventional models. It is evident that there is an asymmetry in the model inputs, with ML models receiving the full set of 128 bins corresponding to the T_2 distribution normalized by ϕ_{NMR}, whereas conventional models rely on only 2 or 6 parameters derived from this distribution. Nevertheless, this contrast reinforces the notion that conventional models tend to be inadequate in complex environments, where additional information is required for accurate modeling. In contrast, ML models, which can handle a large volume of weakly correlated inputs, are able to provide more accurate predictions and capture reservoir nuances, even when based on a single petrophysical dataset.

Accordingly, the comparison between conventional models and ML algorithms in this study should be interpreted along two distinct dimensions: model complexity and informational content. While conventional models operate on a reduced set of parameters derived from the T_2 relaxation-time distribution, ML models exploit the T_2 distribution in its entirety. Therefore, the superior performance observed for ML-based models should not be attributed solely to greater algorithmic flexibility, but mainly to their ability to extract multiscale information embedded in the complete T_2 distribution, which is systematically discarded in conventional approaches. In highly heterogeneous carbonate environments, where multiple relaxation regimes coexist, reduced parametrizations may be inadequate, and the dimensionality reduction imposed by conventional models leads to significant loss of petrophysical information. In this context, ML algorithms act as tools

capable of mapping nonlinear relationships between the full NMR response and permeability, indicating that the predictive gain arises fundamentally from the richer informational content rather than from increased model complexity alone.

Therefore, the superior performance of the MLP model relative to conventional models and ensemble methods should not be interpreted merely because of its greater algorithmic flexibility but rather considering the physical meaning of the information contained in the full T_2 relaxation-time distribution, which the model can generalize. In this sense, the ability of the MLP to integrate information distributed across the entire T_2 spectrum allows the preservation of the multiscale signature of petrophysical heterogeneity in this context, enabling improved permeability predictions due to its strong generalization capability.

The results thus indicate the suitability of using more robust models for the characterization of systems analogous to karstified carbonate reservoirs, with different lithostratigraphic units. The use of laboratory data acquired from core plugs, combined with validation against absolute permeability measurements, contributes to increased modeling reliability and to the correct interpretation of the observed patterns. However, it should be noted that the resolution of the T_2 spectrum has a direct influence on the results, which may affect comparisons with well-log data. Nevertheless, the identified limitations highlight the need to apply these models in other geological contexts and to investigate alternative validation strategies in order to further expand model generalization.

Conclusions

This study demonstrated that the Multi-Layer Perceptron (MLP) neural network model outperformed both conventional and ensemble-based models, mainly due to its lower generalization gap and higher accuracy when evaluated using standard R^2 and RMSE metrics, when applied to highly heterogeneous carbonate rocks. The results confirm that exploiting the full spectrum of T_2 relaxation times is essential for improving predictive accuracy, as it allows a better representation of the multiple pore domains present in these systems. Different portions of the T_2 spectrum may reflect distinct relaxation regimes and provide complementary information about pore-space hierarchy.

From a methodological perspective, this work contributes by adopting a training–test data split strategy guided by geological criteria, preserving lithofacies representativeness and enabling a more realistic assessment of model generalization. The systematic comparison between training and test errors revealed distinct overfitting and underfitting behaviors, highlighting limitations in both conventional models and ensemble-type machine learning algorithms. Future studies should evaluate the transferability of these models across different acquisition conditions, investigation scales, and geological settings, contributing to the advancement of permeability prediction methodologies in highly heterogeneous porous media.

Despite the promising results, some limitations must be acknowledged. The performance of NMR-based models is intrinsically linked to the resolution of the T_2 distribution, which depends on both acquisition conditions and the inversion parameters adopted in laboratory measurements. In addition, the generalization of the models trained in this study to well-log data remains uncertain, since logging measurements differ significantly from laboratory plug measurements in terms of vertical resolution, signal-to-noise ratio, and investigated volume. In this regard, future studies should consider expanding the dataset with a larger number of samples per lithofacies, as well as incorporating additional lithologies, to strengthen the statistical representativeness of the models. The integration of other borehole geophysical data, along with the explicit inclusion of geological parameters as input variables, may further contribute to a more realistic characterization of porous systems.

As future perspectives, the expansion of the dataset to include additional lithofacies and geological contexts is recommended, as well as the integration of complementary information such as digital rock images, quantitative textural parameters, and well-log data, with the aim of enriching the informational content and complexity of the models. Finally, the application and validation of these models on real well-log data represent an essential step toward assessing their operational feasibility and potential impact on petrophysical workflows and the characterization of carbonate reservoirs.

Acknowledgement

This work was partially supported by CAPES (Coordenação de Aperfeiçoamento de Pessoal de Nível Superior) and by the Graduate Program in Geodynamics and Geophysics of the Federal University of Rio Grande do Norte (PPGG-UFRN).

The authors also acknowledge the Núcleo de Processamento de Alto Desempenho (NPAD/UFRN) for providing relevant computational resources, and the Laboratório de Propriedades Físicas das Rochas (LPFR) and Laboratório de Engenharia de Reservatórios de Petróleo (LABRES) for providing the petrophysical data used in this study.

References

Alhakeem, Z.M., Jebur, Y.M., Henedy, S.N., Imran, H., Bernardo, L.F.A., Hussein, H.M.: Prediction of Ecofriendly Concrete Compressive Strength Using Gradient Boosting Regression Tree Combined with GridSearchCV Hyperparameter-Optimization Techniques. Materials. 15, (2022). https://doi.org/10.3390/ma15217432

Araújo, R.E.B., La Bruna, V., Rustichelli, A., Bezerra, F.H.R., Xavier, M.M., Audra, P., Barbosa, J.A., Antonino, A.C.D.: Structural and sedimentary discontinuities control the generation of karst dissolution cavities in a carbonate sequence, Potiguar Basin, Brazil. Mar. Pet. Geol. 123, (2021). https://doi.org/10.1016/j.marpetgeo.2020.104753

Araújo, R.E.B., La Bruna, V., Rustichelli, A., Xavier, M.M., Agosta, F., Bezerra, F.H.R., Brito, M.F.P., Barbosa, J.A., Antonino, A.C.D.: Pore network characteristics as a function of diagenesis: Implications for epigenic karstification in shallow-water carbonates. Mar. Pet. Geol. 149, (2023). https://doi.org/10.1016/j.marpetgeo.2022.106094

Astsauri, T., Habiburrahman, M., Ibrahim, A.F., Wang, Y.: Utilizing machine learning for flow zone indicators prediction and hydraulic flow unit classification. Sci. Rep. 14, (2024). https://doi.org/10.1038/s41598-024-54893-1

Bagni, F.L., Erthal, M.M., Tonietto, S.N., Maia, R.P., Bezerra, F.H., Balsamo, F., Córdoba, V.C., de Souza, F.G., Brod, J.A., Fernandes, C.P., Fonseca, J.P.T.: Karstified layers and caves formed by superposed epigenic dissolution along subaerial unconformities in carbonate rocks – Impact on reservoir-scale permeability. Mar. Pet. Geol. 138, 105523 (2022). https://doi.org/10.1016/j.marpetgeo.2022.105523

Bentéjac, C., Csörgő, A., Martínez-Muñoz, G.: A comparative analysis of gradient boosting algorithms. Artif. Intell. Rev. 54, 1937–1967 (2021). https://doi.org/10.1007/s10462-020-09896-5

Bezerra, F.H., de Castro, D.L., Maia, R.P., Sousa, M.O.L., Moura-Lima, E.N., Rossetti, D.F., Bertotti, G., Souza, Z.S., Nogueira, F.C.C.: Postrift stress field inversion in the Potiguar Basin, Brazil – Implications for petroleum systems and evolution of the equatorial margin of South America. Mar. Pet. Geol. 111, 88–104 (2020). https://doi.org/10.1016/j.marpetgeo.2019.08.001

Bi, J., Ning, L., Zhao, Y., Wu, Z., Wang, C.: Analysis of the Microscopic Evolution of Rock Damage Based on Real-Time Nuclear Magnetic Resonance. Rock Mech. Rock Eng. 56, 3399–3411 (2023). https://doi.org/10.1007/s00603-023-03238-x

Biau, G., Scornet, E.: A random forest guided tour. Test. 25, 197–227 (2016). https://doi.org/10.1007/s11749-016-0481-7

Braga, A.D.P., Ludermir, A.P.D.L.F.D.C., Bernarda, T.: Redes Neurais Artificiais - Teoria e Prática. LTC (2011)

Breiman, L.: Random Forests. (2001)

Carr, H.Y., Purcell, E.M.: Effects of Diffusion on Free Precession in Nuclear Magnetic Resonance Experiments. Physical Review. 94, (1954)

Chang, Y., Zhang, K., Zhang, Y.: New Model for Absolute Permeability Prediction in Coal Samples: Application of Modified Purcell Model to Mercury Injection Pressure and Nuclear Magnetic Resonance Data. ACS Omega. 8, 21120–21132 (2023). https://doi.org/10.1021/acsomega.3c02035

Chen, S., Li, R., Yu, J., Wang, H., Zhang, X.: Study of uncertainties in the inversion algorithms for transverse relaxation distribution. (2010)

Chen, X., Zhao, X., Tahmasebi, P., Luo, C., Cai, J.: NMR-data-driven prediction of matrix permeability in sandstone aquifers. J. Hydrol. (Amst). 618, (2023)(a). https://doi.org/10.1016/j.jhydrol.2023.129147

Chen, X.J., Zhang, R.X., Zhao, X.B., Yang, J.W., Lan, Z.J., Luo, C.F., Cai, J.C.: Multifractal estimation of NMR T2 cut-off value in low-permeability rocks considering spectrum kurtosis: SMOTE-based oversampling integrated with machine learning. Pet. Sci. 20, 3411–3427 (2023)(b). https://doi.org/10.1016/j.petsci.2023.08.001

Chencarek, B., Nascimento, M.S., Souza, A.M., Sarthour, R.S., Santos, B.C.C., Correia, M.D., Oliveira, I.S.: Multi-exponential Analysis of Water NMR Spin–Spin Relaxation in Porosity/Permeability-Controlled Sintered Glass. Appl. Magn. Reson. 50, 211–225 (2019). https://doi.org/10.1007/s00723-018-1050-x

Cipolla, C., Mack, M., Maxwell, S.: Reducing Exploration and Appraisal Risk in Low Permeability Reservoirs Using Microseismic Fracture Mapping-Part 2. (2010)

Cipolla, C.L., Warpinski, N.R., Mayerhofer, M.J., Lolon, E.P., Vincent, M.C.: The Relationship Between Fracture Complexity, Reservoir Properties, and Fracture Treatment Design. (2008)

Coates, G.R., Marschall, D., Mardon, D., Galford, J.: A New Characterization of Bulk-Volume Irreducible Using Magnetic Resonance. SPWLA. 51–63 (1998)

Coates, G.R., Xiao, L., Prammer, M.G.: NMR Logging Principles and Applications. (1999)

Córdoba, V.C.: A evolução da plataforma carbonática Jandaíra durante o Neocretáceo na Bacia Potiguar: Análise paleoambiental, diagenética e estratigráfica, (2001)

Daigle, H., Dugan, B.: An improved technique for computing permeability from NMR measurements in mudstones. J. Geophys. Res. Solid Earth. 116, (2011). https://doi.org/10.1029/2011JB008353

Darcy: Les Fontaines Publiques De la Ville de Dijon: Des Principes a Suivre et des Formules a Employer. , Paris (1856)

Dong, X., Yu, Z., Cao, W., Shi, Y., Ma, Q.: A survey on ensemble learning, (2020)

Dunn, K.J., Bergman, D.J., LaTorraca, G.A.: Nuclear Magnetic Resonance. (2002)

Elkatatny, S., Mahmoud, M., Tariq, Z., Abdulraheem, A.: New insights into the prediction of heterogeneous carbonate reservoir permeability from well logs using artificial intelligence network. Neural Comput. Appl. 30, 2673–2683 (2018). https://doi.org/10.1007/s00521-017-2850-x

Fernandes, A.L., Medeiros, W.E., Bezerra, F.H.R., Oliveira, J.G., Cazarin, C.L.: GPR investigation of karst guided by comparison with outcrop and unmanned aerial vehicle imagery. J. Appl. Geophy. 112, 268–278 (2015). https://doi.org/10.1016/j.jappgeo.2014.11.017

Friedman, J.H.: Greedy Function Aproximation: A Gradient Boosting Machine. The Annals of Statistics. 29, 1189–1232 (2001)

Géron, A.: Mãos à Obra: Aprendizado de Máquina com Scikit-Learn & TensorFlow Conceitos, Ferramentas e Técnicas para a Construção de Sistemas Inteligentes. (2021)

Glover, P.W.J., Zadjali, I.I., Frew, K.A.: Permeability prediction from MICP and NMR data using an electrokinetic approach. Geophysics. 71, (2006). https://doi.org/10.1190/1.2216930

Gonçalves, E.C., da Silva, P.N., Silveira, C.S., Carneiro, G., Domingues, A.B., Moss, A., Pritchard, T., Plastino, A., Azeredo, R.B. de V.: Prediction of carbonate rock type from NMR responses using data mining techniques. J. Appl. Geophy. 140, 93–101 (2017). https://doi.org/10.1016/j.jappgeo.2017.03.014

Hahn, E.L.: Spin Echoes. Physical Review. 80, 580–594 (1950)

Han, Y., Zhou, C., Fan, Y., Li, C., Yuan, C., Cong, Y.: A new permeability calculation method using nuclear magnetic resonance logging based on pore sizes: A case study of bioclastic limestone reservoirs in the A oifield of the Mid-East. Petroleum Exploration and Development. 183–192 (2018)

Haykin, S.S.: Neural Networks and Learning Machines. PRENTICE HALL (2009)

Henrique, B.M., Sobreiro, V.A., Kimura, H.: Literature review: Machine learning techniques applied to financial market prediction. Expert Syst. Appl. 124, 226–251 (2019). https://doi.org/10.1016/j.eswa.2019.01.012

Hinton, G.E., Osindero, S.: A Fast Learning Algorithm for Deep Belief Nets Yee-Whye Teh. (2006)

J Al-Mudhafar, W.: Integrating lithofacies and well logging data into smooth generalized additive model for improved permeability estimation: Zubair formation,

South Rumaila oil field. Marine Geophysical Research. 40, 315–332 (2019). https://doi.org/10.1007/s11001-018-9370-7

Jain, A.K., Mao, J., Mohiuddin, K.M.: Artifical Neural Networks: A Tutorial. (1996)

Jensen, J.L., Flaig, P.P., Hattori, K.E.: The Effects of Facies Variability and Bioturbation Intensity on Permeability in a Mixed Siliciclastic–Carbonate Core from the Upper Strawn Group, Katz Field, Eastern Shelf of the Permian Basin, Texas, USA. Geosciences (Switzerland). 14, (2024). https://doi.org/10.3390/geosciences14120339

Jin, G., Xie, R., Liu, M., Guo, J., Gao, L.: A new method for permeability estimation using integral transforms based on NMR echo data in tight sandstone. J. Pet. Sci. Eng. 180, 424–434 (2019). https://doi.org/10.1016/j.petrol.2019.05.056

Kang, W.L., Zhou, B.B., Issakhov, M., Gabdullin, M.: Advances in enhanced oil recovery technologies for low permeability reservoirs, (2022)

Kellal, S., Nandito, D., El-Husseiny, A., Hassan, A., Hanafy, S.M.: Machine learning-driven permeability prediction in carbonates and sandstones using NMR relaxation data. Artificial Intelligence in Geosciences. 7, (2026). https://doi.org/10.1016/j.aiig.2026.100193

Kenyon, W.E., Day, P.I., Straley, C., Willemsen, J.F.: A Three-Part Study of NMR Longitudinal Relaxation Properties of Water-Saturated Sandstones. SPE Formation Evaluation. 622–636 (1988)

Klinkenberg, L.J.: The Permeability of Porous Media to Liquids and Gases. (1941)

Liang, Z., Li, X., Sun, A., Hou, F., Zhai, Z., Sui, Q.: Nuclear Magnetic Resonance Logging-Based Permeability Classification Modeling for Tight Sandstone Reservoirs. Processes. 12, (2024). https://doi.org/10.3390/pr12071309

Ling, H.E., Lun, Z., Li, J., Ji, M.A., Lui, R., Shuqin, W., Zhao, W.: Complex relationship between porosity and permeability of carbonate reservoirs and its controlling factors: A case study of platform facies in Pre-Caspian Basin. (2014)

Liu, J., Fan, Y., Qiu, T., Ge, X., Deng, S., Xing, D.: A novel pulse sequence and inversion algorithm of three-dimensional low field NMR technique in unconventional resources. Journal of Magnetic Resonance. 303, 67–74 (2019). https://doi.org/10.1016/j.jmr.2019.04.009

Liu, Y., Wang, Y., Zhang, J.: New Machine Learning Algorithm: Random Forest. (2012)

Lopes, J.A.G.: Impactos da Dissolução Cárstica na Permo-Porosidade de Rochas Carbonáticas: Implicações para o Desenvolvimento de Redes de Fraturas Alargadas de Camadas Super-K, (2022)

Lopes, J.A.G., Medeiros, W.E., Oliveira, J.G., Santana, F.L., Araújo, R.E.B., La Bruna, V., Xavier, M.M., Bezerra, F.H.R.: Three-dimensional characterization of karstic dissolution zones, fracture networks, and lithostratigraphic interfaces using GPR cubes, core logs, and petrophysics: Implications for thief zones development in carbonate reservoirs. Mar. Pet. Geol. 150, (2023). https://doi.org/10.1016/j.marpetgeo.2023.106126

Lu, T., Li, Z., Zhou, Y., Zhang, C.: Enhanced Oil Recovery of Low-Permeability Cores by SiO2 Nanofluid. Energy and Fuels. 31, 5612–5621 (2017). https://doi.org/10.1021/acs.energyfuels.7b00144

Mahdaviara, M., Rostami, A., Shahbazi, K.: State-of-the-art modeling permeability of the heterogeneous carbonate oil reservoirs using robust computational approaches. Fuel. 268, (2020). https://doi.org/10.1016/j.fuel.2020.117389

Mahesh, B.: Machine Learning Algorithms - A Review. International Journal of Science and Research (IJSR). 9, 381–386 (2020). https://doi.org/10.21275/art20203995

Masroor, M., Emami Niri, M., Rajabi-Ghozloo, A.H., Sharifinasab, M.H., Sajjadi, M.: Application of machine and deep learning techniques to estimate NMR-derived permeability from conventional well logs and artificial 2D feature maps. J. Pet. Explor. Prod. Technol. 12, 2937–2953 (2022). https://doi.org/10.1007/s13202-022-01492-3

Matos, R.M.D. De: The Northeast Brazilian Rift System. Tectonics. 11, 766–791 (1992)

Mayr, A., Binder, H., Gefeller, O., Schmid, M.: The evolution of boosting algorithms: From machine learning to statistical modelling. Methods Inf. Med. 53, 419–427 (2014). https://doi.org/10.3414/ME13-01-0122

McCulloch, W.S., Pitts, W.: A Logical Calculus of the Ideas Immanent in Nervous Activity. , Chicago (1943)

Meiboom, S., Gill, D.: Modified spin-echo method for measuring nuclear relaxation times. Review of Scientific Instruments. 29, 688–691 (1958). https://doi.org/10.1063/1.1716296

Natekin, A., Knoll, A.: Gradient boosting machines, a tutorial. Front. Neurorobot. 7, (2013). https://doi.org/10.3389/fnbot.2013.00021

Neto, O. da C.P., Manoel Soares, U., Gedson Fernandes da Silva, J., Henrique Roesner, E., Pires Florencio, C., Augusto Valentin de Souza, C.: Bacia Potiguar. (2007)

Otchere, D.A., Ganat, T.O.A., Ojero, J.O., Tackie-Otoo, B.N., Taki, M.Y.: Application of gradient boosting regression model for the evaluation of feature selection techniques in improving reservoir characterisation predictions. J. Pet. Sci. Eng. 208, (2022). https://doi.org/10.1016/j.petrol.2021.109244

Pedregosa, F., Buitinck, L., Louppe, G., Grisel, O., Varoquaux, G., Mueller, A.: Scikit-learn. GetMobile: Mobile Computing and Communications. 19, 29–33 (2015). https://doi.org/10.1145/2786984.2786995

Prieto-González, L.S., Agulles-Pedrós, L.: Exploring the Potential of Machine Learning algorithms to Improve Diffusion Nuclear Magnetic Resonance Imaging Models Analysis. (2023)

Radwan, A.E., Trippetta, F., Kassem, A.A., Kania, M.: Multi-scale characterization of unconventional tight carbonate reservoir: Insights from October oil filed, Gulf of Suez rift basin, Egypt. J. Pet. Sci. Eng. 197, (2021). https://doi.org/10.1016/j.petrol.2020.107968

Rezaee, R.: Synthesizing Nuclear Magnetic Resonance (NMR) Outputs for Clastic Rocks Using Machine Learning Methods, Examples from North West Shelf and Perth Basin, Western Australia. Energies (Basel). 15, (2022). https://doi.org/10.3390/en15020518

Rostami, A., Kordavani, A., Parchekhari, S., Hemmati-Sarapardeh, A., Helalizadeh, A.: New insights into permeability determination by coupling Stoneley wave propagation and conventional petrophysical logs in carbonate oil reservoirs. Sci. Rep. 12, (2022). https://doi.org/10.1038/s41598-022-15869-1

Sagi, O., Rokach, L.: Ensemble learning: A survey, (2018)

Samuel, A.L.: Some Studies in Machine Learning Using the Game of Checkers. (1959)

Sander, R., Pan, Z., Connell, L.D.: Laboratory measurement of low permeability unconventional gas reservoir rocks: A review of experimental methods, (2017)

Segal, M.R.: UCSF Recent Work Title Machine Learning Benchmarks and Random Forest Regression Publication Date Machine Learning Benchmarks and Random Forest Regression. (2003)

Silva, O.L., Bezerra, F.H.R., Maia, R.P., Cazarin, C.L.: Karst landforms revealed at various scales using LiDAR and UAV in semi-arid Brazil: Consideration on karstification processes and methodological constraints. Geomorphology. 295, 611–630 (2017). https://doi.org/10.1016/j.geomorph.2017.07.025

Souza, A., Carneiro, G., Zielinski, L., Polinski, R., Schwartz, L., Hürlimann, M.D., Boyd, A., Helton Rios, E., Coutinho Camilo dos Santos, B., Andrighetto Trevizan, W., de França Machado, V., Bagueira de Vasconcellos Azeredo, R.: Permeability Prediction Improvement Using 2D NMR Diffusion-T2 Maps. (2013)

Sun, X., Opulencia, M.J.C., Alexandrovich, T.P., Khan, A., Algarni, M., Abdelrahman, A.: Modeling and optimization of vegetable oil biodiesel production with heterogeneous nano catalytic process: Multi-layer perceptron, decision regression tree,

and K-Nearest Neighbor methods. Environ. Technol. Innov. 27, (2022). https://doi.org/10.1016/j.eti.2022.102794

Tiab, Djebbar., Donaldson, E.C..: Petrophysics : theory and practice of measuring reservoir rock and fluid transport properties. Elsevier (2024)

Tikhonov, A.N., Arsenin, V.Y.: Solutions of Ill-Posed Problems. (1963)

Wei, C., Zheng, J.: Thief Zone Characterization and its Impact on Well Performance Based on Surveillance Data, Experimental Data and Theoretical Analysis for a Carbonate Reservoir. (2019)

Wolpert, David.H.: The Lack of A Priori Distinctions Between Learning Algorithms. Neural Comput. 8, (1996)

Xu, Z.X., Li, S.Y., Li, B.F., Chen, D.Q., Liu, Z.Y., Li, Z.M.: A review of development methods and EOR technologies for carbonate reservoirs, (2020)

Yu, H., Wang, Z., Wen, F., Rezaee, R., Lebedev, M., Li, X., Zhang, Y., Iglauer, S.: Reservoir and lithofacies shale classification based on NMR logging. Petroleum Research. 5, 202–209 (2020). https://doi.org/10.1016/j.ptlrs.2020.04.005

Zhang, T., Tang, M., Ma, Y., Zhu, G., Zhang, Q., Wu, J., Xie, Z.: Experimental study on CO2/Water flooding mechanism and oil recovery in ultralow - Permeability sandstone with online LF-NMR. Energy. 252, (2022). https://doi.org/10.1016/j.energy.2022.123948

Zhang, Y., Haghani, A.: A gradient boosting method to improve travel time prediction. Transp. Res. Part C Emerg. Technol. 58, 308–324 (2015). https://doi.org/10.1016/j.trc.2015.02.019

Zhao, J., Wang, Q., Rong, W., Zeng, J., Ren, Y., Chen, H.: Permeability Prediction of Carbonate Reservoir Based on Nuclear Magnetic Resonance (NMR) Logging and Machine Learning. Energies (Basel). 17, (2024). https://doi.org/10.3390/en17061458

Zhao, Y., Zhu, G., Dong, Y., Danesh, N.N., Chen, Z., Zhang, T.: Comparison of low-field NMR and microfocus X-ray computed tomography in fractal characterization of pores in artificial cores. Fuel. 210, 217–226 (2017). https://doi.org/10.1016/j.fuel.2017.08.068

Zhu, L., Zhang, L., Wei, C., Zhou, Y., Huang, X., Zhang, Y.: Inversion of the permeability of a tight gas reservoir with the combination of a deep Boltzmann kernel extreme learning machine and nuclear magnetic resonance logging transverse relaxation time spectrum data. (2017)

Zounemat-Kermani, M., Batelaan, O., Fadaee, M., Hinkelmann, R.: Ensemble machine learning paradigms in hydrology: A review, (2021)

Appendix A

Variations of GridSearchCV applied to select the best models for each algorithm, with Table 1 referring to the ensemble methods and Table 2 to the neural network models.

Table 1 - Range of chosen hyperparameters RFR and GBR

Hyperparameters	Variations RFR	Variations GBR
n_estimators	512 to 7936	512 to 10240
criterion	“squared_error” or “absolute_error”	“squared_error” or “absolute_error”
max_depth	“None”, or values 1 to 5	“None”, or values 1 to 5
min_samples_split	[1,2,3,4]	[1,2,3,4]
min_samples_leaf	[1,2,3,4]	[1,2,3,4]
learning_rate	X	True or False
tol	X	0.0001 or 0.00001
loss	X	0.1, 0.05 and 0.01
alpha	X	0.9, 0.75 and 0.5
bootstrap	True or False	True or False
max_features	None or “log2”	None or “log2”

Table 2 - Range of chosen hyperparameters MLP

Hyperparameters	Variations
activation	“tanh” or “relu”
alpha	0.001 or 0.0001
beta_1	0.9 or 0.8
beta_2	0.999 or 0.9
epsilon	1e-08 or 1e-09
hidden_layer_sizes	1, 2 or 3 hidden layers, with 32 to 1024 perceptrons in each layer.
learning_rate	“constante” or “adaptative”
learning_rate_init	0.01 or 0.001
n_iter_no_change	100 or 10
solver	“sgd” or “adam”
tol	1e-03 or 1e-04 or 1e-05

Appendix B

Model coefficients and the optimal set of hyperparameters for permeability modeling for each model (Table 1).

Table 1 - The number of hyperparameter combinations used, the hours needed to train, and the best hyperparameter combination

Model	Training combinations	Training Time (hours)	Model Coefficients and Best Hyperparameters
SDR	X	X	**a:** 7.2; **b:** 2.7; **c:** 0.41
Han	X	X	**a:** 13.59; **b:** 2.43; **c:** 0.05; **d:** 0.07; **e:** 1.05; **f:** -0.02
Random Forest Regressor	12.180	108,93	**n_estimators:** 742; **criterion:** squared_error; **max_depht:** "5; **min_samples_split:** 3; **min_samples_leaf:** 1; **bootstrap**: True; **max_features:** None.
Gradient Boosting Regressor	47.880	462,72	**n_estimators:** 1024; **criterion:** friedman_mse; **max_depth:** "5; **min_samples_split:** 2; **min_samples_leaf:** 3; **learning_rate:** 0.1; **tol:** 0.0001; **loss:** absolute_error; **alpha:** 0.9; **bootstrap**: True; **max_features:** None.
Multi-Layer Perceptron	2.348	108, 13	**activation:** "tanh"; **alpha:** 0.01; **beta_1**: 0.9; **beta_2**: 0.9; **epsilon**: 1e-08; **hidden_layer_sizes**: (32, 64, 64); **learning_rate**: "constant"; **learning_rate_init**: 0.001; **solver:** "adam"; **n_ter_no_change**: 100; **tol:** 0.001